

Fe–N/C catalysts synthesized by heat-treatment of iron triazine carboxylic acid derivative complex for oxygen reduction reaction

 Cite this: *RSC Adv.*, 2014, 4, 12168

 Qian Cui,^{†a} Shujun Chao,^{†ab} Panhao Wang,^a Zhengyu Bai,^a Huiying Yan,^a Kui Wang^a and Lin Yang^{*a}

4,4',4''-s-Triazine-1,3,5-triyltri-*p*-aminobenzoic acid (H₃TATAB) was used as a ligand to prepare an iron–TATAB (Fe–TATAB) complex for the development of an effective oxygen reduction reaction (ORR) catalyst. The activity of the catalyst depended on weight ratios between the Fe–TATAB complex and carbon black and heat-treated temperatures. The results showed that the Fe–N_{70%}/C-800 catalyst (the weight ratio of Fe complex to carbon black was 70 : 30 and the catalyst was pyrolyzed at 800 °C) had good catalytic activity toward ORR with the onset potential at 0.91 V vs. RHE and a kinetic current density of 4.3 mA cm⁻² at 0.6 V vs. RHE in alkaline medium. Moreover, the Fe–N_{70%}/C-800 catalyst had better tolerance to methanol crossover effect in comparison with commercial Pt/C (20%). The morphology and composition of the catalysts were characterized by high resolution transmission electron microscopy (HRTEM), X-ray diffraction (XRD) as well as X-ray photoelectron spectroscopic (XPS). The electrocatalytic activities were demonstrated by cyclic voltammetry (CV), linear sweep voltammetry (LSV), chronoamperometric measurements and stability accelerated tests. According to rotating disk electrode (RDE) measurements and Koutecky–Levich analysis, the overall electron transfer number in the catalyzed ORR was found to be 3.7–3.9 and the ORR process was mainly a four-electron pathway. The results indicate that the Fe–N_{70%}/C-800 catalyst may be a promising cathode catalyst for ORR.

 Received 9th September 2013
 Accepted 16th January 2014

DOI: 10.1039/c3ra44958k

www.rsc.org/advances

1. Introduction

Fuel cells are quite promising as clean energy converting devices to replace traditional energy devices.^{1,2} The cathode oxygen reduction reaction (ORR) is a crucial step due to its sluggish kinetics, and therefore, acceleration of the ORR is necessary to enhance the performance of fuel cells.^{3,4} Platinum (Pt) is the most active element for the ORR, so a high loading of Pt or Pt-based alloys are usually used as the cathode catalysts in order to accelerate the ORR.^{5–7} However, the high cost and scarcity of Pt hinder the commercial implementation of fuel cells.^{8,9} To reduce the cost, intensive research efforts have been made to find out a suitable substitute for Pt.^{10–12} Non-precious metal catalysts (NPMCs) are probably the best option based on a long-term and sustainable solution.

In 1964, Jasinski firstly reported the ORR catalytic activity of cobalt phthalocyanine.¹³ Later studies indicated that the activity and stability of transition metal macrocycles could be enhanced by pyrolysis.¹⁴ A significant breakthrough was achieved years later when Yeager and co-workers showed that the presence of the macrocyclic structure was not essential to the ORR activity.¹⁵ Therefore, other kinds of NPMCs for ORR such as transition metal chalcogenides, metal oxides/carbides/nitrides and conductive polymer-based catalysts, have been developed in recent years.^{16,17} Among the different kinds of NPMCs, pyrolyzed carbon supported transition metal–nitrogen complexes (M–N_x/C) are considered to be the most promising ORR catalysts for their high activity and long-term stability.^{18–20} According to previous literature, four necessary factors must coexist to obtain a high performance catalyst for ORR, which are transition metal, nitrogen precursor, carbon support and heat-treatment.^{19,21} The metal (M) ions used in this type of catalyst are mainly Fe and Co, which can give the most active metallic centers.^{22,23} Recently, Wang *et al.* synthesized a Co-corrole/C catalyst using corrole as a macrocyclic ligand and cobaltous acetate as a metal precursor. Although the catalyst had a high catalytic performance, the synthesis procedure was quite complex.²⁴ Moreover, it is generally believed that traditional nitrogen-containing macrocyclic ligands (such as porphyrin

^aSchool of Chemistry and Chemical Engineering, Key Laboratory of Green Chemical Media and Reactions, Ministry of Education, Collaborative Innovation Center of Henan Province for Fine Chemicals Green Manufacturing, Henan Normal University, Xinxiang 453007, P.R. China. E-mail: yanglin1819@163.com; Fax: +86-373-3328507; Tel: +86-373-3325058

^bDepartment of Chemistry, Xinxiang Medical University, Xinxiang 453007, P.R. China
[†] These authors contributed equally to this work and should be considered co-first authors.

and phthalocyanine) are costly,^{25,26} hence, selecting a more cost-effective ligand is crucial for ORR catalysts.

Studies have shown that the most commonly used coordination ligands as the nitrogen sources are bipyridine, polypyrrole, polyaniline as well as phenanthroline, and so on.^{21,23,27,28} It seems fairly certain that the activity of the M–N_x/C catalyst is related to its nitrogen content and type of ligands.²⁹ 4,4',4''-s-Triazine-1,3,5-triyltri-*p*-aminobenzoic acid (H₃TATAB) is a kind of nitrogen-rich triazine carboxylic acid ligand, and the synthesis process is quite simple.³⁰ Recently, H₃TATAB has been reported to bridge metal cations (Cu or Zn) in a well-defined three-dimensional structure to form metal–organic frameworks (MOFs).³¹ The facts have attracted intense interest in various research areas such as heterogeneous catalysis, chemical sensors, ion exchange and gas storage. However, there are only a few researches that reported triazine carboxylic acid ligands used for ORR. In view of the high nitrogen content and low cost of H₃TATAB, we synthesized an efficient Fe–N/C catalyst using H₃TATAB as a nitrogen-rich ligand for ORR. HRTEM, XRD as well as XPS were used for the morphology and structural characterization. The activities of the catalysts were then tested in alkaline solution using CV, LSV, chronoamperometric measurements and stability accelerated tests.

2. Experimental sections

2.1 Materials

Ferrous chloride tetrahydrate (FeCl₂·4H₂O), *N,N*-dimethylformamide (DMF) and absolute ethanol were purchased from China National Pharmaceutical Group Corp. Commercial 20% Pt/C catalyst was obtained from Alfa Aesar. Vulcan XC-72 (carbon black) was obtained from Cabot and used as a catalyst support. All chemical reagents used in this study were of analytical grade and were used as received without further purification. Double distilled water (DD water) was used throughout the experiments.

2.2 Catalyst preparation

H₃TATAB was synthesized according to previous literature.³⁰ 0.486 g obtained H₃TATAB was added to 40 mL DMF to form a clear solution and stirred for 30 min at room temperature, which was a deprotonation step. Afterward, 0.099 g FeCl₂·4H₂O was dispersed in the above solution by ultrasonic treatment for 30 min. The product was stirred for 4 h at 30 °C and 1 mL 30% H₂O₂ was added to end the reaction. This suspension was stirred for another 10 min and dried with a rotary vacuum evaporator at 90 °C for 1 h. Then, 0.07 g resulting product and 0.03 g carbon black were dispersed in 40 mL absolute ethanol with ultrasonic treatment for 30 min and constant stirring for 10 h at room temperature. The resulting black mixture was filtered and rinsed with DD water and absolute ethanol several times, and dried in a vacuum at 40 °C overnight. The resulting powder was ground in a mortar and placed in a tube furnace, and pyrolyzed at 800 °C for 120 min at a rate of 3 °C min⁻¹ under a nitrogen atmosphere. The obtained catalyst was denoted as Fe–N_{70%}/C-800.

2.3 Characterization

The morphology of the catalysts was measured by a JEOL-100CX HRTEM operated at 200 kV. The crystallographic phases and purity information of the prepared samples were characterized by XRD, and the corresponding XRD patterns were recorded on a Bruker D & Advance X-ray diffractometer with a Cu K α radiation source ($\lambda = 1.5406 \text{ \AA}$). XPS measurements were performed on an MULTILAB2000 instrument using a monochromic Al X-ray source.

2.4 Electrochemical measurement

The electrochemical measurements were carried out in a three-electrode cell using a CHI660 D electrochemical workstation. A glass carbon rotating disk electrode (RDE) coated with the catalyst was used as the working electrode, a saturated calomel electrode (SCE) as the reference electrode, and a Pt wire as the counter electrode. All measured potentials were converted into the values referring to a reversible hydrogen electrode (RHE). Before the catalyst was loaded to the glassy carbon disk, the electrode was polished mechanically with γ -aluminite powder under an abrasive paper to obtain a mirror-like surface, washed with DD water and absolute ethanol and allowed to dry at room temperature. The working electrode was prepared as follows: 2 mg catalyst was added into 1 mL ethanol and 40 μ L 5 wt% perfluorosulfonic acid, which was dispersed by ultrasonication for approximately 10 min to obtain a homogeneous suspension. Next, 18 μ L of the dispersion was uniformly dispersed on a freshly polished glassy carbon electrode (4.0 mm in diameter) and dried under the lamp. The catalyst loading on the glassy carbon electrode was 0.27 mg cm⁻². By using the same electrode configuration, the same loading of commercial Pt/C (20%) modified electrode was prepared in the same way for comparison. Current densities were calculated by the ratio of current and the geometric surface area of working electrode.

The electrochemical experiments were carried out in O₂ saturated 0.1 M KOH electrolyte. The cyclic voltammograms were recorded with a scan rate of 50 mV s⁻¹ in the potential range 0 to 1.2 V vs. RHE. RDE measurements were conducted at different rotating speeds from 400 to 2500 rpm with a scan rate of 10 mV s⁻¹. All electrochemical experiments were performed at 25 \pm 1 °C.

3. Results and discussion

Details of the formation mechanism of the Fe–N/C catalysts are shown in Fig. 1. As illustrated by Fig. 1, the Fe–N/C catalysts were prepared by a three-step strategy. Firstly, the Fe–TATAB complex was synthesized *via* Fe²⁺ coordinating with H₃TATAB. Secondly, the Fe–TATAB complex was mixed with carbon black with different weight ratios. At last, the Fe–N/C catalysts were acquired by the pyrolysis of carbon supported Fe–TATAB complex in flowing nitrogen. In order to find the most appropriate proportion of Fe–TATAB to carbon black and the pyrolysis temperature, different Fe complex to carbon weight ratios (20 : 80, 40 : 60, 60 : 40, 70 : 30 and 80 : 20) were synthesized and pyrolyzed at 600 °C, 800 °C and 1000 °C under a nitrogen

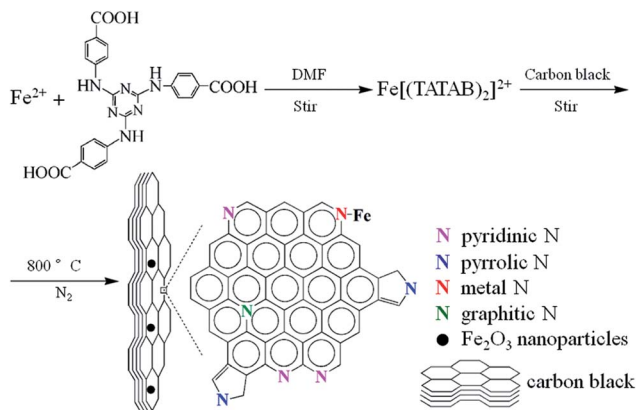


Fig. 1 Schematic diagram of the synthesis of Fe-N/C samples.

atmosphere, respectively. The following electrochemical measurements indicated that Fe-N_{70%}/C-800 was the most active ORR catalyst among all the synthesized samples. Therefore, the Fe-N_{70%}/C-800 catalyst was mainly discussed in the present work. According to the HRTEM, XRD and XPS analysis results, the carbon supported Fe-TATAB complex was decomposed into Fe₂O₃ nanoparticles, pyridinic N (26.9 at% in total doped nitrogen), metal-N (15.9 at%), graphitic N (23.7 at%) and pyrrolic N (33.6 at%). In order to study the role of Fe₂O₃ in the ORR, the Fe-N_{70%}/C-800 catalyst was pre-leached in 4 M hydrochloric acid at 80 °C for 6 h to remove Fe₂O₃ nanoparticles.

3.1 Physical characterization

Fig. 2a shows the typical TEM image of the Fe-N_{70%}/C catalyst pyrolyzed at 800 °C. These nanoparticles exhibit a *d* spacing of 0.2516 nm, corresponding to the (311) plane of Fe₂O₃, as shown by the HRTEM image in Fig. 2b. Because the content of Fe₂O₃ is low, twelve TEM images were taken to perform the histogram of particle size distribution. The average size of Fe₂O₃ nanoparticles was calculated to be approximately 31 nm in Fig. 2c.

The crystallographic phases and purity information of the prepared samples were characterized by XRD. Fig. 3a presents the XRD patterns of the Fe-TATAB complex, carbon black and Fe-N_{70%}/C samples before and after heat-treatment at different temperatures. In Fig. 3a, the peaks at 16.8° and 26.2° are attributed to the Fe-TATAB complex, while the peak at 24.8° is assigned to carbon black. The result shows the crystallographic phase of carbon black doesn't change with and without heat-treatment. After pyrolysis, the characteristic diffraction peaks

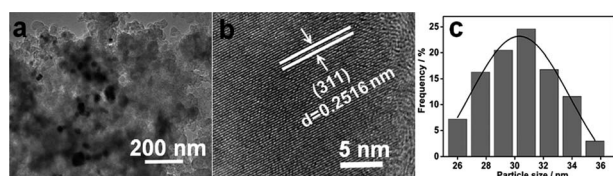


Fig. 2 (a) TEM image, (b) HRTEM image and (c) histogram of particle size distribution of the Fe-N_{70%}/C-800 catalyst.

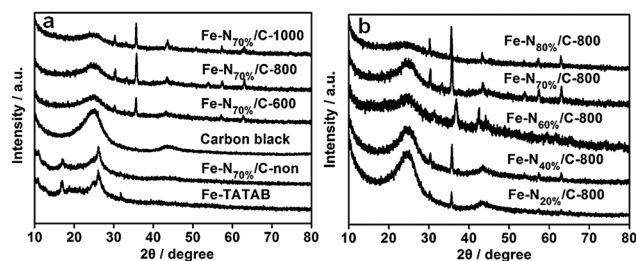


Fig. 3 XRD patterns of (a) Fe-TATAB complex, carbon black and Fe-N_{70%}/C samples before and after heat-treatment at different temperatures; (b) the Fe-N/C-800 samples synthesized with different Fe complex to carbon black mass ratios.

of the Fe-TATAB complex disappear due to decomposition of the Fe-TATAB complex. Comparing samples with and without heat-treatment, several characteristic diffraction peaks are observed after heat-treatment. Fig. 3b shows the XRD patterns of the Fe-N/C samples synthesized at different mass ratios after pyrolysis at 800 °C. In all the XRD patterns, the wide peak located at about 2θ of 25° can be assigned to the carbon support.³² The diffraction peaks at the 2θ values of 30.24°, 35.63°, 43.28°, 57.27° and 62.93° are attributed to maghemite Fe₂O₃ (220), (311), (400), (511) and (440) crystalline facet, respectively (JCPDS Card no. 39-1346). These results indicate that part of the carbon supported Fe-TATAB complex has decomposed into iron oxide during the heat-treatment process. In addition, the magnitude of crystalline peaks of Fe₂O₃ increases with increasing Fe-TATAB loading from 20 to 70%. With a further increase of the complex loading (up to 80%), the shape of these peaks becomes weak and narrow, which indicates the presence of a high amount of Fe₂O₃ in the Fe-N_{70%}/C-800 sample.

In order to obtain information about the surface atomic composition of the samples, XPS analysis was performed for the unpyrolyzed sample and the sample heat-treated at 800 °C. Due to the fact that the most abundant elements on the sample surface were Fe, N, C and O, XPS analysis in the binding energy region of each element was carried out. The relative atomic percentages of Fe, N, C and O are 0.43, 6.28, 80.98 and 12.31 in the unpyrolyzed sample, meanwhile, the Fe-N_{70%}/C-800 catalyst shows the relative atomic percentages are 0.53, 1.2, 91.88 and 6.41, respectively. Fig. 4a and b present the Fe 2p spectral region for the unpyrolyzed sample and the sample heat-treated at 800 °C, respectively. Two bands can be observed, which correspond to lower energy (Fe 2p_{3/2}) and higher energy (Fe 2p_{1/2}) asymmetric bands originated from the spin-orbital splitting. The peaks at 711.2 and 724.9 eV from Fig. 4a and b can be attributed to Fe 2p_{3/2} and Fe 2p_{1/2}, respectively. According to the literature, the standard Fe 2p_{3/2}/Fe 2p_{1/2} signals corresponding to metallic iron, ferrous and ferric states are located at 706.7/719.8, 709.2/722.8 and 711.2/724.8 eV, respectively.³³ It can be concluded that the ferric state is the dominant species on the two samples. The presence of Fe(III) should be due to the conversion of Fe(II) irons coming from the starting material used in the synthesis. These Fe³⁺ species can be bonded with oxygen or nitrogen to form Fe(III)-N_x or Fe(III) oxides,^{3,34} which agree well with the XRD results.

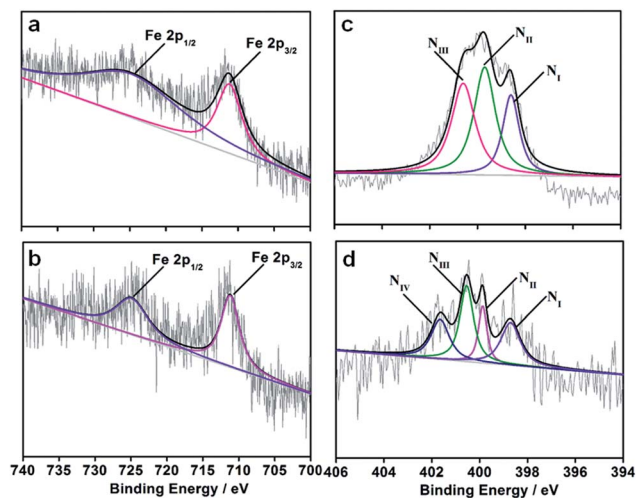


Fig. 4 XPS spectra of Fe 2p for the Fe-N_{70%}/C sample before (a) and after (b) heat-treatment at 800 °C, N 1s for the Fe-N_{70%}/C sample before (c) and after (d) heat-treatment at 800 °C.

For the unpyrolyzed sample in Fig. 4c, the N 1s band can be separated into three contributions (N_I, N_{II} and N_{III}) with binding energies of 398.6, 399.7 and 400.6 eV, respectively. The lower energy band of N_I can be attributed to nitrogen atoms in the triazine rings and the energy band of N_{III} can be attributed to the nitrogen atoms bonded to the edges of the rings in the form of 2C-NH.^{35,36} The N_{II} band at 399.7 eV should be attributed to metal-N bonds.^{33,37} For the sample pyrolyzed at 800 °C in Fig. 4d, the N1s band can be converted into four peaks (N_I, N_{II}, N_{III} and N_{IV}) with binding energies of 398.7, 399.7, 400.5 and 401.6 eV, which can be attributed to pyridinic N, metal-N, pyrrolic N and graphitic N, respectively. It is found that 26.9 at% N from pyridinic N, 15.9 at% from metal-N, 23.7 at% from graphitic N and 33.6 at% from pyrrolic N. Studies show that pyridinic N, graphitic N and metal-N_x are possible active sites, which are conducive to improve the ORR activity and stability.^{33,37}

In comparison with Fig. 5a and b, it is found that the relative content of C-N single bonds is obviously increased after pyrolysis. In all cases, five bands can be observed, which are marked as C_I, C_{II}, C_{III}, C_{IV} and C_V, respectively. The dominant contributions are the C_I signal at 284.6 eV for the C sp² bonds in the graphitic domains or the aromatic structure.^{24,27} The peak of C_{II} at 285.4 eV for the C sp³ bonds could be assigned to that in the amorphous carbon substrate or in the C-N single bonds formed during the pyrolysis. Obviously, the C_{II} band of the catalyst pyrolyzed at 800 °C is sharper and broader than that of the unpyrolyzed sample, which is ascribed to additional C-N single bonds formed during the pyrolysis. The C_{III} band at 286.4 eV and the C_{IV} band at 288.0 eV could be assigned to the C=N bonds and the C-O single bonds which exist on the carbon black surface, respectively. Finally, the broader C_V band at the binding energy region of 290.7 eV could be assigned to the C=O bonds of different materials such as carbonyl and carboxyl, which reside on the carbon substrate.³³

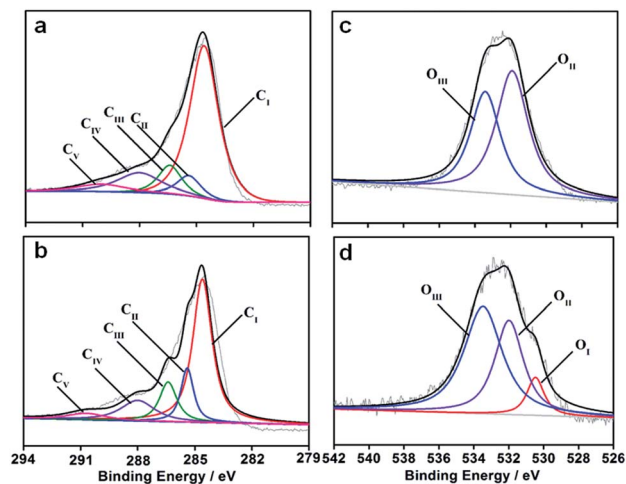


Fig. 5 XPS spectra of C 1s for the Fe-N_{70%}/C sample before (a) and after (b) heat-treatment at 800 °C, O 1s for the Fe-N_{70%}/C sample before (c) and after (d) heat-treatment at 800 °C.

The results of the O 1s spectral region are presented in Fig. 5c and d for both the unpyrolyzed and pyrolyzed samples. The corresponding spectra deconvoluted into three contributions are noted as O_I, O_{II}, and O_{III}, respectively. The O_I band at the lower binding energy of 530 eV could be assigned to oxygen which is bonded to Fe to form Fe₂O₃ or other oxides.^{33,38} The O_{II} band at the binding energy of 531.6 eV could be related to oxygen in C=O bonds. The O_{III} band at 533.5 eV may be assigned to C-OH or C-O-C groups in carboxylic, epoxy or phenol groups on the carbon surface. Compared with Fig. 5c and d, the appearance of O_I is probable due to the formation of small amounts of Fe₂O₃ nanoparticles after the pyrolysis, which is consistent with previous HRTEM and XRD results.

3.2 Electrochemical characterization

To evaluate the electrocatalytic activity of the Fe-N/C catalysts, CV experiments choosing Fe-N_{70%}/C-800 were tested through a conventional three-electrode method in O₂ or N₂ saturated 0.1 M KOH aqueous solutions (Fig. 6a). Despite the capacitive background, a characteristic ORR peak appears at *ca.* 0.77 V vs. RHE in the O₂ saturated electrolyte, while no significant response is observed in the oxygen-absent medium, indicating the effective electrochemical reduction of oxygen initiated on the Fe-N_{70%}/C-800 catalyst. To further investigate the ORR performance, we carried out the LSV measurements on a RDE for each of the electrode materials in O₂ saturated 0.1 M KOH at a scan rate of 10 mV s⁻¹ and a rotation rate of 1600 rpm. It is worth mentioning that onset potential and kinetic current density are two essential parameters that represent the kinetic and thermodynamic characteristics of the catalytic reaction. Fig. 6b shows the ORR polarization curves of the Fe-N_{70%}/C samples synthesized at different heat-treatment temperatures and commercial Pt/C (20%). The onset potential increases from 0.87 to 0.91 V vs. RHE with increasing heat-treatment temperature, indicating that the Fe-TATAB complex might form several bonds such as Fe-N_x and C-N with the carbon support during the heat

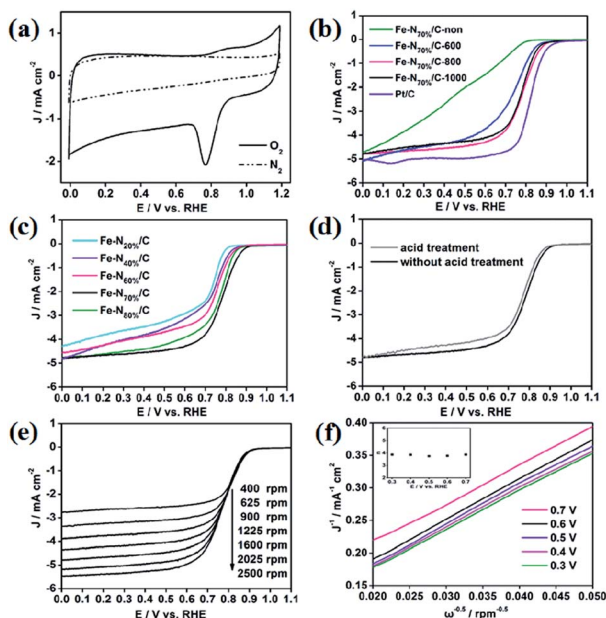


Fig. 6 Catalytic activity towards electrochemical reduction of oxygen in 0.1 M KOH at $25 \pm 1^\circ\text{C}$. (a) CVs of the Fe-N_{70%}/C-800 catalyst in O₂ and N₂-saturated 0.1 M KOH solution at a scan rate of 50 mV s⁻¹; (b) LSVs of the Fe-N_{70%}/C samples synthesized at different heat-treatment temperatures and commercial Pt/C (20%) with a scan rate of 10 mV s⁻¹ and a rotation rate of 1600 rpm; (c) LSVs of Fe-N/C-800 samples with different mass ratios; (d) LSVs of the Fe-N_{70%}/C-800 catalyst with and without acid treatment. (e) LSVs of the Fe-N_{70%}/C-800 catalyst at various rotation rates; (f) Koutecky–Levich plots for the Fe-N_{70%}/C-800 catalyst obtained from LSVs in (e) at different potentials; inset showing the distribution graph of transferred electron number.

treatment, facilitating the electron transfer from the carbon support to O₂.²³ The same trend could also be observed in the kinetic current density, which increases from 3.7 to 4.1 mA cm⁻² at 0.6 V vs. RHE. With a further increase in temperature up to 1000 °C, the onset potential remains the same while the kinetic current density declines slightly. These observations indicate that the optimal pyrolysis temperature is around 800 °C. The LSV of commercial Pt/C (20%) gives the onset potential at 0.95 V vs. RHE and the kinetic current density of 4.9 mA cm⁻² at 0.6 V vs. RHE. The results indicate that the catalytic activity of Fe-N_{70%}/C-800 is very close to commercial Pt/C (20%). The Fe-N_{70%}/C catalyst before heat-treatment indicates some activity. The activity may be attributed to Fe-N_x bond and carbon support, because triazine has no activity towards ORR. Fig. 6c further investigates the effect of Fe-TATAB content on the activity of the Fe-N/C-800 samples. With the increasing of Fe-TATAB complex loading from 20 to 70 wt%, the onset potential of the Fe-N/C-800 samples positively shifted and the kinetic current density for the ORR increases. Further increasing the complex loading up to 80 wt%, the activity of the Fe-N_{80%}/C-800 drops dramatically. It is indisputable that the Fe-N_{70%}/C-800 catalyst has a better ORR catalytic activity than other samples. Fig. 6d shows LSVs of the Fe-N_{70%}/C-800 catalyst with and without acid treatment. Compared with the Fe-N_{70%}/C-800 catalyst without acid treatment, the onset potential has a little negative shift and the

current density decreases slightly, which suggests that Fe₂O₃ doesn't play a critical role in the ORR. However, according to the previous work, an appropriate amount of iron oxide could promote the enhancement of N-doping during the synthesis procedure.^{39,40} In our work, the Fe-N_{70%}/C-800 with a high amount of Fe₂O₃ was the most active ORR catalyst among all the synthesized samples. Therefore, the Fe₂O₃ obtained during the pyrolysis process may facilitate N-doping in carbon and further increase the catalytic activity for ORR.

Fig. 6e shows the RDE polarization curves for ORR on the Fe-N_{70%}/C-800 catalyst modified electrode with various rotation rates from 400 to 2500 rpm. ORR occurs under mixed kinetic-diffusion control at high potential regions, followed by a plateau of the diffusion limiting current, which increases with the rotation rate due to the increase of the oxygen diffusion through the electrode surface. The transferred electron number per oxygen molecule involved in the ORR process was evaluated using the below Koutecky–Levich (K-L) equation:⁴¹

$$1/j = 1/j_k + 1/(B\omega^{1/2})$$

where j represents the measured current density, j_k is the kinetic current density, and ω is the angular velocity of the electrode. B could be calculated from the slope of K-L plots based on the Levich equation as follows:

$$B = 0.62nFCD^{2/3} \nu^{-1/6}$$

where n is the number of electrons transferred, F is the Faraday constant ($F = 96485 \text{ C mol}^{-1}$), C is the concentration of O₂ gas in 0.1 M KOH solution ($C = 1.2 \times 10^{-6} \text{ mol cm}^{-3}$), D is the diffusion coefficient of O₂ gas ($D = 1.9 \times 10^{-5} \text{ cm}^2 \text{ s}^{-1}$), and ν is the kinematic viscosity of 0.1 M KOH solution ($\nu = 0.01 \text{ cm}^2 \text{ s}^{-1}$). Fig. 6f depicts the K-L plots of the Fe-N_{70%}/C-800 catalyst at various potentials from 0.3 to 0.7 V vs. RHE. There is a good linearity between j^{-1} and $\omega^{-1/2}$ over the examined potential range. The numbers of electrons transferred per O₂ molecule (n) are calculated to be 3.7–3.9 from the slope of the K-L plots (inset in Fig. 6f). The results suggest that the ORR is mainly a four-electron and one-step process to generate H₂O.

As an ORR electrocatalyst for fuel cells, a high catalytic selectivity for cathode reactions against fuel oxidation is important. The Fe-N_{70%}/C-800 catalyst has a better stability and tolerance to methanol crossover effect than commercial Pt/C (20%) by the chronoamperometric measurements. In Fig. 7a, the Fe-N_{70%}/C-800 catalyst exhibits a strong and stable amperometric response after the introduction of 10 vol% methanol, suggesting a remarkably good tolerance to methanol crossover effect. For Pt/C (20%), however, the current instantaneously jumped to positive values once adding methanol to the electrolyte at 4000 s, indicating a poor tolerance to methanol crossover effect. The results imply that the Fe-N_{70%}/C-800 catalyst modified electrode has a good selectivity for ORR when methanol coexists. The durability of the Fe-N_{70%}/C-800 and Pt/C (20%) catalysts are also measured through current–time measurements at 0.7 V vs. RHE (Fig. 7b). Only ca. 4% current reduction is observed on the Fe-N_{70%}/C-800 catalyst after

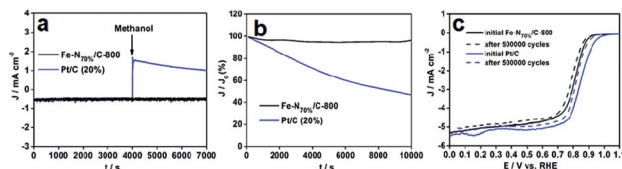


Fig. 7 (a) Current–time chronoamperometric response of the Fe-N_{70%}/C-800 catalyst and commercial Pt/C (20%). The arrow indicates the introduction of 10 vol% methanol; (b) the chronoamperometric measurements for the ORR on the Fe-N_{70%}/C-800 catalyst and commercial Pt/C (20%) at 0.7 V vs. RHE. The measurements were performed in O₂ saturated 0.1 M KOH solution; (c) polarization curves on Fe-N_{70%}/C-800 and Pt/C catalysts at 1600 rpm in O₂-saturated 0.1 M KOH electrolyte before and after 50 000 potential cycles with a scan rate of 10 mV s⁻¹. The potential cycles were from 0.6 to 1.05 V vs. RHE in O₂-saturated 0.1 M KOH solution at room temperature with a scan rate of 50 mV s⁻¹.

10 000 s, whereas Pt/C loses more than 50% of its initial activity, which also confirms a better stability of ORR on the Fe-N_{70%}/C-800 catalyst than that on commercial Pt/C (20%) in alkaline environment. In order to evaluate the stability rigorously, the durability of the Fe-N_{70%}/C-800 catalyst was investigated by stability accelerated tests consisting of 50 000 cycles in O₂ saturated 0.1 M KOH electrolyte at a scan rate of 50 mV s⁻¹ between 0.6 and 1.05 V vs. RHE.^{42,43} Durability data of the Fe-N_{70%}/C-800 catalyst is provided in Fig. 7c along with that of commercial Pt/C (20%) for comparison. Fe-N_{70%}/C-800 shows a slight decrease of 0.018 V vs. RHE in the half-wave potential, while Pt/C shows a potential decrease of 0.03 V vs. RHE. Moreover, the current densities obtained at 0.2 V vs. RHE before and after 50 000 cycles for Fe-N_{70%}/C-800 show no obvious difference (0.1 mA cm⁻²) while the difference for Pt/C is 0.27 mA cm⁻². Overall, the Fe-N_{70%}/C-800 catalyst shows comparable durability with the commercial Pt/C catalyst under the studied conditions.

According to the previous literature,^{40,44–47} the onset potential of Fe-N/C-based catalysts is in the range 0.7 to 0.99 V vs. RHE. In contrast, our synthesized Fe-N_{70%}/C-800 catalyst has a better onset potential of 0.91 V vs. RHE. The stability and tolerance to methanol crossover effect of the Fe-N_{70%}/C-800 catalyst are comparable with other Fe-N/C-based catalysts.

4. Conclusion

In summary, we have successfully synthesized a novel Fe-N/C catalyst using H₃TATAB as the nitrogen precursor, ferrous chloride as the iron precursor and carbon black as the catalyst support. From HRTEM, XRD and XPS analysis, Fe₂O₃ nanoparticles were obtained after heat-treatment of the carbon supported Fe-TATAB complex, which promoted the enhancement of N-doping during the synthesis procedure. The weight ratios of the Fe-TATAB complex to carbon black and heat-treated temperature strongly influenced the activity of the Fe-N/C catalyst. The Fe-N_{70%}/C-800 catalyst was an efficient electrocatalyst for the ORR with the onset potential at 0.91 V vs. RHE and the kinetic current density of 4.3 mA cm⁻² at 0.6 V vs. RHE

in 0.1 M KOH solution. The catalyst exhibited a high electrochemical activity, long-term stability and tolerance to methanol crossover effect. The performance of the Fe-N_{70%}/C-800 catalyst is close to that of commercial Pt/C (20%), which makes it a very promising electrocatalyst for fuel cells.

Acknowledgements

This work was financially supported by the National Natural Science Foundation of China (grant no. 21301051) and Innovative Research Team in University (grant no. IRT 1061).

Notes and references

- 1 Y. H. Bing, H. S. Liu, L. Zhang, D. Ghosh and J. J. Zhang, *Chem. Soc. Rev.*, 2010, **39**, 2184.
- 2 R. Li, Z. D. Wei, X. L. Gou and W. Xu, *RSC Adv.*, 2012, **3**, 9978.
- 3 Y. Zhao, K. Watanabe and K. Hashimoto, *J. Am. Chem. Soc.*, 2012, **134**, 19528.
- 4 S. J. Guo, S. Zhang, L. H. Wu and S. H. Sun, *Angew. Chem., Int. Ed.*, 2012, **51**, 11770.
- 5 B. A. Kakade, H. L. Wang, T. Tamaki, H. Ohashi and T. Yamaguchi, *RSC Adv.*, 2013, **3**, 10487.
- 6 Y. Zhang, C. Ma, Y. M. Zhu, R. Si, Y. Cai, J. X. Wang and R. R. Adzic, *Catal. Today*, 2013, **202**, 50.
- 7 S. I. Choi, S. F. Xie, M. H. Shao, J. H. Odell, N. Lu, H. C. Peng, L. Protsailo, S. Guerrero, J. Park, X. H. Xia, J. G. Wang, M. J. Kim and Y. N. Xia, *Nano Lett.*, 2013, **13**, 3420.
- 8 Z. Peng and H. Yang, *J. Am. Chem. Soc.*, 2009, **131**, 7542.
- 9 M. H. Shao, K. Sasaki and R. R. Adzic, *J. Am. Chem. Soc.*, 2006, **128**, 3526.
- 10 Y. Y. Liang, Y. G. Li, H. L. Wang, J. G. Zhou, J. Wang, T. Regier and H. J. Dai, *Nat. Mater.*, 2011, **10**, 780.
- 11 X. G. Li, G. Liu and B. N. Popov, *J. Power Sources*, 2010, **195**, 6373.
- 12 G. Liu, X. G. Li, P. Ganesan and B. N. Popov, *Appl. Catal., B*, 2009, **93**, 156.
- 13 R. Jasinski, *Nature*, 1964, **201**, 1212.
- 14 H. Jahnke, M. Schönborn and G. Zimmermann, *Top. Curr. Chem.*, 1976, **61**, 133.
- 15 J. Zagal, P. Bindra and E. Yeager, *J. Electrochem. Soc.*, 1980, **127**, 1506.
- 16 D. Susac, A. Sode, L. Zhu, P. C. Wong, M. Teo, D. Bizzotto, K. A. R. Mitchell, R. R. Parsons and S. A. Campbell, *J. Phys. Chem. B*, 2006, **110**, 10762.
- 17 Y. J. Feng, A. Gago, L. Timperman and N. Alonso-Vante, *Electrochim. Acta*, 2011, **56**, 1009.
- 18 R. L. Liu, C. Malotki, L. Arnold, N. Koshino, H. Higashimura, M. Baumgarten and K. Müllen, *J. Am. Chem. Soc.*, 2011, **133**, 10372.
- 19 L. Ding, J. L. Qiao, X. F. Dai, J. Zhang, J. J. Zhang and B. L. Tian, *Int. J. Hydrogen Energy*, 2012, **37**, 14103.
- 20 Z. W. Chen, D. Higgins, A. P. Yu, L. Zhang and J. J. Zhang, *Energy Environ. Sci.*, 2011, **4**, 3167.
- 21 M. Lefèvre, E. Proietti, F. Jaouen and J. P. Dodelet, *Science*, 2009, **324**, 71.

- 22 F. Charreteur, S. Ruggeri, F. Jaouen and J. P. Dodelet, *Electrochim. Acta*, 2008, **53**, 6881.
- 23 C. W. B. Bezerra, L. Zhang, K. C. Lee, H. S. Liu, A. L. B. Marques, E. P. Marques, H. J. Wang and J. J. Zhang, *Electrochim. Acta*, 2008, **53**, 4937.
- 24 H. C. Huang, I. Shown, S. T. Chang, H. C. Hsu, H. Y. Du, M. C. Kuo, K. T. Wong, S. F. Wang, C. H. Wang, L. C. Chen and K. H. Chen, *Adv. Funct. Mater.*, 2012, **22**, 3500.
- 25 A. Morozan, S. Campidelli, A. Filoramo, B. Joussetme and S. Palacin, *Carbon*, 2011, **49**, 4839.
- 26 Z. F. Ma, X. Y. Xie, X. X. Ma, D. Y. Zhang, Q. Z. Ren, N. Heß-Mohr and V. M. Schmidt, *Electrochem. Commun.*, 2006, **8**, 389.
- 27 J. L. Qiao, L. Xu, L. Ding, L. Zhang, R. Baker, X. F. Dai and J. J. Zhang, *Appl. Catal., B*, 2012, **125**, 197.
- 28 G. Wu, K. L. More, C. M. Johnston and P. Zelenay, *Science*, 2011, **332**, 443.
- 29 J. T. Wang, S. Li, G. W. Zhu, W. Zhao, R. X. Chen and M. Pan, *J. Power Sources*, 2013, **240**, 381.
- 30 Q. R. Fang, D. Q. Yuan, J. L. Sculley, J. R. Li, Z. B. Han and H. C. Zhou, *Inorg. Chem.*, 2010, **49**, 11637.
- 31 K. F. Babu, M. A. Kulandainathan, I. Katsounaros, L. Rassaei, A. D. Burrows, P. R. Raithby and F. Marken, *Electrochem. Commun.*, 2010, **12**, 632.
- 32 L. Ding, Q. Xin, X. J. Zhou, J. L. Qiao, H. Li and H. J. Wang, *J. Appl. Electrochem.*, 2013, **43**, 43.
- 33 A. Velázquez-Palenzuela, L. Zhang, L. C. Wang, P. L. Cabot, E. Brillas, K. Tsay and J. J. Zhang, *J. Phys. Chem. C*, 2011, **115**, 12929.
- 34 S. Jiang, C. Z. Zhu and S. J. Dong, *J. Mater. Chem. A*, 2013, **1**, 3593.
- 35 Y. C. Zhao, Z. Liu, W. G. Chu, L. Song, Z. X. Zhang, D. L. Yu, Y. J. Tian, S. S. Xie and L. F. Sun, *Adv. Mater.*, 2008, **20**, 1777.
- 36 H. Zhao, L. Pan, J. Jin, L. Li and J. Xu, *Fuel Cells*, 2012, **12**, 876.
- 37 R. Kothandaraman, V. Nallathambi, K. Artyushkova and S. C. Barton, *Appl. Catal., B*, 2009, **92**, 209.
- 38 L. Ding, X. F. Dai, R. Lin, H. J. Wang and J. L. Qiao, *J. Electrochem. Soc.*, 2012, **159**, 577.
- 39 Z. S. Wu, S. B. Yang, Y. Sun, K. Parvez, X. L. Feng and K. Müllen, *J. Am. Chem. Soc.*, 2012, **134**, 9082.
- 40 C. H. Choi, S. H. Park and S. I. Woo, *Int. J. Hydrogen Energy*, 2012, **37**, 4563.
- 41 G. F. Dong, M. H. Huang and L. H. Guan, *Phys. Chem. Chem. Phys.*, 2012, **14**, 2557.
- 42 K. A. Kuttiyiel, K. Sasaki, Y. M. Choi, D. Su, P. Liu and R. R. Adzic, *Energy Environ. Sci.*, 2012, **5**, 5297.
- 43 J. X. Wang, C. Ma, Y. M. Choi, D. Su, Y. M. Zhu, P. Liu, R. Si, M. B. Vukmirovic, Y. Zhang and R. R. Adzic, *J. Am. Chem. Soc.*, 2011, **133**, 13551.
- 44 Z. P. Li, Z. X. Liu, K. N. Zhu, Z. Li and B. H. Liu, *J. Power Sources*, 2012, **219**, 163.
- 45 L. Wang, J. Yin, L. Zhao, C. G. Tian, P. Yu, J. Q. Wang and H. G. Fu, *Chem. Commun.*, 2013, **49**, 3022.
- 46 X. G. Fu, Y. R. Liu, X. P. Cao, J. T. Jin, Q. Liu and J. Y. Zhang, *Appl. Catal., B*, 2013, **130**, 143.
- 47 S. M. Zhang, H. Y. Zhang, Q. Liu and S. L. Chen, *J. Mater. Chem. A*, 2013, **1**, 3302.